Sensitivity Analysis

Oliwer Sliczniuk[a,*], Pekka Oinas[a]

[a]Aalto University, School of Chemical Engineering, Espoo, 02150, Finland

ARTICLE INFO

Keywords:
Supercritical extraction
Sensitivity analysis
Mathematical modelling

ABSTRACT

This study aimed to investigate the supercritical extraction process of caraway oil from caraway seeds. The extraction was performed in a partially filled extractor with a fixed bed operated under multiple operating conditions. A distributed-parameter model describes the fluid-solid extraction process with CO_2 as a solvent. The concept of quasi-one-dimensional flow is applied to reduce the number of spatial dimensions. The flow is assumed to be uniform across any cross-section, although the area available for the fluid phase can vary along the extractor. The local sensitivity analysis investigates the influence of infinitely small changes in the inlet temperature, pressure, and flow rate on the extraction yield.

1. Introduction

The present study focuses on extracting essential oil from the caraway (Carum carvi L.) seeds with supercritical fluid extraction and modelling that process. Caraway is a biennial plant belonging to the Apiaceae family. It is widespread in Asia, Europe, and North Africa. The essential oil obtained from caraway finds its potential application as a fragrance ingredient in perfumes, liquors, and toothpaste. As presented by Hromis et al. [1], the dried caraway contains nearly 2.8–5% essential oil, from which the main compounds are carvone, pinene, camphene, limonene, and carveol.

The economic feasibility of the process is crucial when selecting the appropriate technology. Conventional processes, such as distillation and organic solvent extraction, are frequently used for essential oil extraction. The distillation process is carried out at a high temperature, which causes thermal degradation of thermolabile compounds—considering that alternative techniques like supercritical fluid extraction gained popularity for extraction. Supercritical carbon dioxide, in particular, is attractive due to its unique properties such as inflammable, non-toxic, low critical temperature and non-corrosive. Furthermore, its critical point is relatively low compared to other fluids, making it a suitable alternative to traditional extraction techniques. The supercritical fluids exhibit both gas- and liquid-like properties so that operating conditions can adjust the dissolving power.

Various mathematical models have been proposed to describe the extraction of valuable compounds from a fixed biomass bed. However, selecting an appropriate extraction model requires understanding the physical phenomena occurring in the operational unit. Each model has its own set of assumptions and describes different mass transfer mechanisms and equilibrium relationships.

One model proposed by Reverchon et al. [2] is the hot ball model, which is based on an analogy to heat transfer and describes an extraction process from solid particles containing small quantities of solute where solubility is not a limiting factor.

Another model, the Broken-and-Intact Cell model, was presented by Sovova [3]. This model describes a system where the outer surfaces of particles have been mechanically interrupted, allowing easy access of solvent to the solute from the broken cells. In contrast, the solute from the intact cells is less accessible due to high mass transfer resistance.

Reverchon [4] developed a model for fluid-solid extraction, where the oil is treated as a single component, and the extraction process is controlled by internal mass transfer resistance, neglecting external mass transfer. However, this model does not consider the influence of axial dispersion or changes in fluid density and flow rate along the bed.

In this work, the fundamental governing equations are derived and combined with the kinetic model suggested by Reverchon [4] to obtain a general model for the oil extraction process from the caraway seed. This model simplifies some of the physical behaviour to obtain a control-oriented model. It is assumed that the extraction process operates semi-continuously in a cylindrical vessel. The solvent is first brought to supercritical conditions, pumped through a fixed bed of finely chopped biomass, and the solute is extracted from the biomass. The solvent and solute are then separated in a flush drum, and the extract is collected. The feed flow rate (F_{in}) and inlet temperature (T_{in}) of the extractor can be measured and manipulated, while the vessel pressure (P) can also be measured and manipulated. However, the outlet temperature (T_{out}) can only be measured. Figure 1 shows a simplified flow diagram.

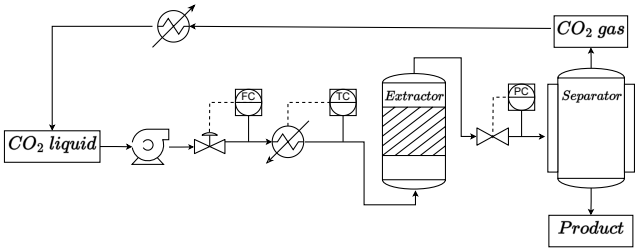

Figure 1: Process flow diagram

*Corresponding author
oliwer.sliczniuk@aalto.fi (O. Sliczniuk)
ORCID(s): 0000-0003-2593-5956 (O. Sliczniuk); 0000-0002-0183-5558 (P. Oinas)

This study aims to develop a process model for extracting natural substances from solid materials and liquids using supercritical fluids, specifically supercritical CO_2. To achieve this, the solvent properties are estimated based on thermodynamic relations and the extraction kinetic parameters estimated based on a set of experiments conducted at various conditions. The maximum likelihood estimator is used to solve the parameter estimation problem, and the obtained parameters are subjected to regression to derive correlations. These correlations enable the process model to be generalized across a range of temperatures (40 to 50 $°C$) and pressures (200 to 300 bar).

The study is structured as follows: Chapter 2.1 provides a general discussion on supercritical fluids to familiarize the reader with their properties. Chapter 2.2 introduces the general balance equations. The balance equations are combined with the extraction kinetic equation to develop the process model in Chapter 2.3. The maximum likelihood technique is presented in Chapter **??** and is then combined with the process model. Chapter **??** describes the experimental work and the data collected from experiments, which are used to estimate missing parameters related to the extraction kinetic. Finally, the parameter estimations and simulation results are discussed in Chapters 3 and 4

2. Materials and methods

2.1. Supercritical fluids

A supercritical fluid (SCF) is a substance at a temperature and pressure above its critical point, where there are no distinct liquid and gas phases but below the pressure required to compress it into a solid. SCFs can move through porous solids like gases, which is faster than liquid transport through such materials. SCFs have a higher ability to dissolve materials like liquids or solids compared to gases. Near the critical point, small changes in pressure or temperature result in significant changes in density, allowing many properties of an SCF to be fine-tuned. By changing the pressure and temperature, the properties of carbon dioxide can be tuned to be more liquid-like or gas-like.

Fluid properties can be divided into two kinds: equilibrium properties and transport properties. The equation of state can be used accurately to predict the equilibrium properties, such as fluid density, enthalpy, vapour pressure, fugacity and fugacity coefficient, vapour-liquid equilibrium, and all kinds of excess properties.

Supercritical CO_2's thermodynamic properties, such as density or specific heat capacity, vary significantly with slight changes in temperature and pressure due to real gas effects. The Peng-Robinson equation of state (P-R EOS) is used to calculate the thermodynamic properties by accounting for these real gas effects are presented in Appendix **??**. The P-R EOS belongs to a specific class of thermodynamic models for modelling the pressure of a solvent as a function of temperature and density and which can be rewritten as a cubic function of the molar volume.

To determine the thermodynamic properties of a real gas, it is necessary to evaluate the departure function of the chosen equation of state for that property. As explained by Elliott [5], the departure function describe the difference between the actual value of a thermodynamic property of a real gas and its value if the gas were ideal under the same temperature and pressure conditions. The ideal gas serves as a reference state to which the properties of real gases are compared. The departure function measures the extent to which a real gas deviates from ideal gas behaviour. The departure functions allow for the accurate calculation of thermodynamic properties for real gases.

The properties of CO_2 are presented as a function of operating conditions (temperature and pressure) in Figure 2. At standard atmospheric pressure and temperature, CO_2 behaves as an ideal gas, and its compressibility factor equals unity. However, at high pressures and/or low temperatures, intermolecular forces between gas molecules become more significant, causing them to deviate from ideal behaviour. As a result, the compressibility factor can be greater than or less than unity, depending on the magnitude of these forces. As presented in Figure 2a, the compressibility factor obtained from the Peng-Robinson equation of state varies strongly depending on the operating conditions.

The real gas effects are also visible on the density plot presented in Figure 2b. The density calculations are based on the compressibility factor, and its value depends on the operating conditions. The fluid properties near the critical point are unique and combine gas-like and liquid-like properties. The details of calculations are explained in Appendix **??**.

Figure 2c show the behaviour of the heat capacity of a supercritical fluid at constant pressure (C_p). The details of the calculations can be found in Appendix **??**. Contrary to the density, which varies monotonically, the specific heat shows very high levels in a narrow region. In the subcritical region, the phase transition is associated with an effective spike in the heat capacity (i.e., the latent heat). Approaching the critical point, the latent heat falls to zero, which is accompanied by a gradual rise in heat capacity in the pure phases near phase transition. At the critical point, the latent heat is zero, but the heat capacity shows a diverging singularity. Beyond the critical point, there is no divergence, but rather a peak in the heat capacity; the highest point of this peak identifies the Widom line (as discussed by Simeoni et al. [6] and Banuti [7]).

Figure 2d represent how the specific enthalpy change with the operating conditions. The details of calculations are discussed in Appendix **??**.

Transport properties such as viscosity and conductivity play a crucial role in engineering design for production, fluid transportation, and processing. However, as highlighted by Sheng et al. [8], developing a satisfactory theory for transport properties of real dense gases and liquids is a challenging task. This is due to the inherent difficulties involved in accurate measurements and the complexity involved in theoretical treatments.

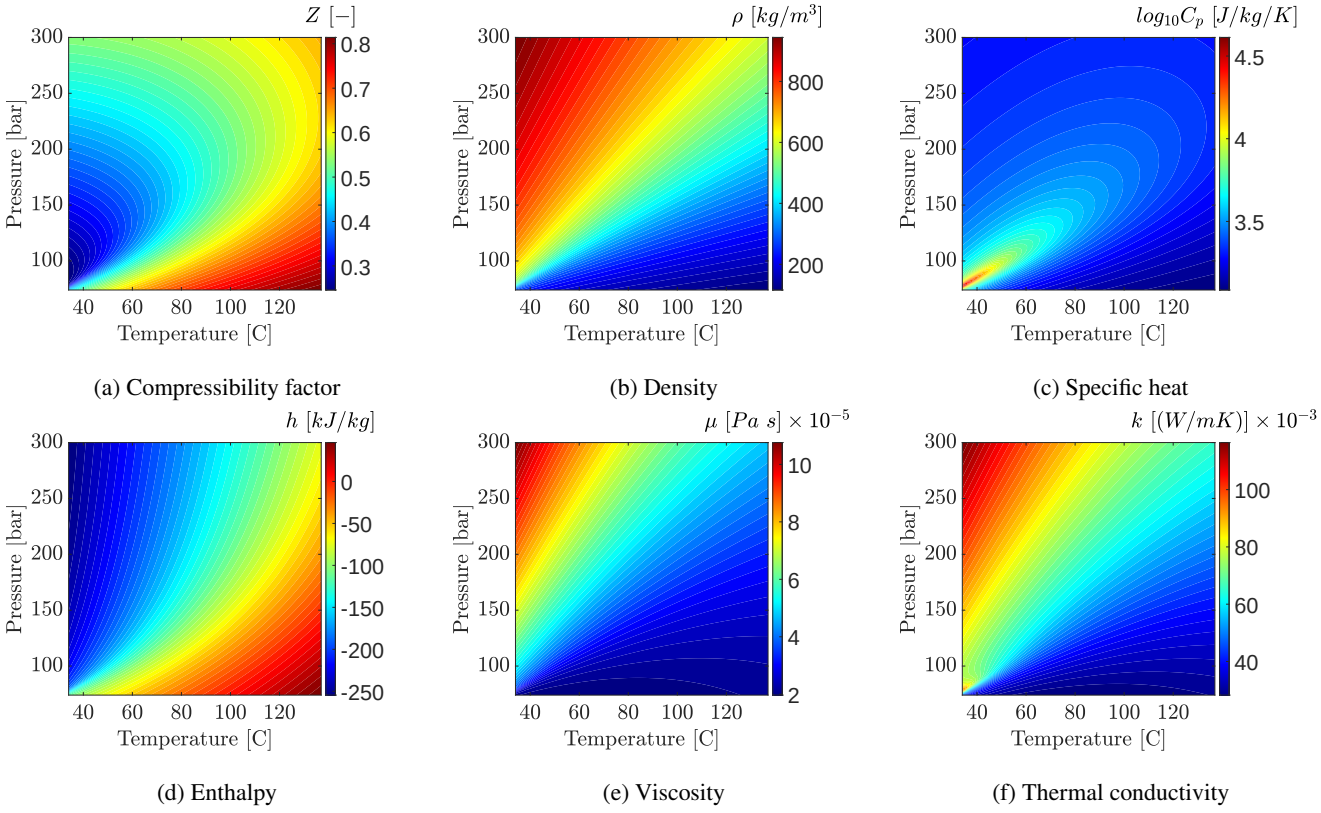

(a) Compressibility factor (b) Density (c) Specific heat

(d) Enthalpy (e) Viscosity (f) Thermal conductivity

Figure 2: Properties of CO_2 based on the equation of state and correlations

To address this issue, the correlations of transport coefficients are either empirical or based on some theoretical foundation. Chapman-Enskog's theory (presented in Chapman and Cowling [9]) for transport properties of dense gases based on the distribution function is a popular theoretical approach. However, the Chapman-Enskog theory was developed for rigid spherical molecules and modifications are required to apply it to real gases. Many correlations have been proposed following the Chapman-Enskog theory in the form of reduced density and reduced temperature, such as those developed by Fenghour et al. [10], and Laesecke and Muzny [11] from the National Institute of Standards and Technology (NIST). The correlation of Laesecke and Muzny [11] is presented in Figure 2e.

NIST has developed a viscosity formulation consisting of four contributions: (i) for the limit of zero density, (ii) for the initial density dependence, (iii) for the residual viscosity, and (iv) for the singularity of the viscosity at the critical point. The NIST correlation covers temperatures from 100 to 2000 K for gaseous CO_2, and from 220 to 700 K with pressures along the melting line up to 8000 MPa for compressed and supercritical liquid states. These correlations and theories are essential in predicting transport properties for real gases and liquids and can assist in engineering design and analysis.

Similarly, the NIST developed the correlation, which describe the behaviour of thermal diffusivity of CO_2. The work of Huber et al. [12] captures the singular behaviour of thermal conductivity around the critical point. The correlation is applicable for the temperature range from the triple point to 1100 K and pressures up to 200 MPa. Figure 2f shows how the thermal conductivity of carbon dioxide change depending on the operating conditions.

2.2. Governing equations

The governing equation for a quasi-one-dimensional compressible flow in Cartesian coordinates can be found in the Appendix **??** and in the work of Anderson [13]. Quasi-one-dimensional flow is a fluid flow characterized by the assumption that the flow properties remain uniform across any given cross-section of the flow. This assumption is made when there is a variation in the cross-sectional area of the flow channel, such as an irregular shape or partial filling of an extractor. In such cases, the flow is considered to be quasi-one-dimensional because the velocity and other flow properties are assumed to vary only in the direction of flow.

The quasi-one-dimensional compressible Navier-Stokes equations in Cartesian coordinates are given by Equations 1 to 3. The derivation of these Equations are presented in Appendix **??**.

$$\frac{\partial\left(\rho_f A_f(z)\right)}{\partial t}+\frac{\partial\left(\rho_f A_f(z) v\right)}{\partial z}=0 \tag{1}$$

$$\frac{\partial\left(\rho_f v A_f(z)\right)}{\partial t}+\frac{\partial\left(\rho_f A_f(z) v^2\right)}{\partial z}=-A_f(z)\frac{\partial P}{\partial z} \tag{2}$$

$$\frac{\partial\left(\rho_f e A_f(z)\right)}{\partial t}+\frac{\partial\left(\rho_f A_f(z) v e\right)}{\partial z}=-P\frac{\left(A_f(z) v\right)}{\partial z}+\frac{\partial}{\partial z}\left(\frac{\partial T}{\partial z}\right) \tag{3}$$

where ρ_f is the density of the fluid, $A_f(z)$ is the function which describe change of the cross-section, v is the velocity, P is the total pressure, e is the internal energy of the fluid, t is time and z is the spacial direction.

Based on governing equations, the small discontinuity (defined as δ) in flow properties, shown in Figure 3, can be analysed. The analysis follows the work of Schreier [14].

	ρ_f	$\rho_f+\delta\rho_f$	
$v\rightarrow$	P	$P+\delta P$	$v+\delta v\rightarrow$
	T	$T+\delta T$	

Figure 3: Small discontinuity in one-dimensional flow

The discontinuity is presumed to be at rest relative, and the balance equations become

$$\rho_f\delta v+v\delta\rho_f+\delta\rho_f\delta v=0$$
$$\delta P=\delta v\delta\rho_f$$

These relations are equally valid if the two regions are separated by a region of finite width rather than a discontinuity.

$$\lim_{\rho_f v\rightarrow 0}\rho_f\delta v+v\delta\rho_f+\delta\rho_f\delta v=0/\delta\rho_f\rightarrow\frac{dv}{d\rho_f}=-\frac{v}{\rho_f}$$

By combining the momentum equation with the above equation, we get

$$\frac{dv}{d\rho_f}=-\frac{dv}{dP}\frac{dP}{d\rho_f}=-\frac{1}{\rho v}\frac{dP}{d\rho_f}=-\frac{v}{\rho_f} \tag{4}$$

Suppose the flow is presumed to be isentropic, $dP/d\rho_f = c^2$, so $v^2 = c^2$, where c is the speed of sound. This can be interpreted as a small pressure wave propagating with the speed of sound relative to the flow. Moreover, if the flow velocity is relatively low, all pressure changes are hydrodynamic (due to velocity motion) rather than thermodynamic which leads to $\partial\rho_f/\partial P \approx 0$. In other words, the small changes in pressure due to flow velocity changes do not change the density.

2.3. Extraction model

2.3.1. Continuity equation

The obtained above quasi-one-dimensional continuity equation (Equation 1) is further modified by specifying a function $A_f(z) = A\phi(z)$ to take into account the change of the cross-section available for the fluid. The Equation 5 shows the differential form of the continuity equation:

$$\frac{\partial(\rho_f(T(t,z),P(t))\phi(z))}{\partial t}+\frac{\partial(\rho_f(T(t,z),P(t))vA\phi(z))}{\partial z}=0 \tag{5}$$

where A is the total cross-section of the extractor and $\phi(z)$ describe porosity along the extractor.

Assuming that the mass flow rate is constant in time, the temporal derivative becomes zero, and the spatial derivative can be integrated along z as

$$\int\frac{\partial(\rho_f(T(t,z),P(t))vA\phi(z))}{\partial z}dz=0\rightarrow F=\rho_f(T(t,z),P(t))vA\phi(z) \tag{6}$$

Here, F is a constant obtained from the integration and is understood as the mass flux per unit area, which is assumed to be constant along z. To simplify the dynamics of the system, it is assumed that $F = F(t)$ is a control variable and affects the whole system instantaneously. This assumption allows for finding the velocity profile that satisfies mass continuity based on $F(t)$, $\phi(z)$, and $\rho_f(T(t,z),P(t))$.

$$v=\frac{F(t)}{\rho_f(T(t,z),P(t))A\phi(z)} \tag{7}$$

The fluid density $\rho_f(T(t,z),P(t))$ can be obtained from an equation of state if temperature and the thermodynamic pressure (assumed $P(t)$ to be constant along z due to the low-Mach number condition) are known. The variation in density may be caused by the fluid accumulation in the system (equivalent to pressure change), which occurs instantaneously along z or by a temperature change.

Analogously, the superficial velocity might be introduced to the model and defined as

$$u=v\phi(z)=\frac{F(t)}{\rho_f(T(t,z),P(t))A} \tag{8}$$

2.3.2. Mass balance for the fluid phase

The detailed derivation of the mass balance equation for the fluid phase can be found in Appendix **??**. The movement of the pseudo-homogeneous fluid phase (Equation 9) is considered only in the axial direction due to quasi-one-dimensional assumptions, which take into account variation of the void fraction. Furthermore, the thermodynamic pressure is assumed to be constant along the device as presented by Equation 4. Additionally, the boundary layer adjacent to the inner wall of the extractor is neglected, resulting in a constant velocity profile across any cross-section of the extractor perpendicular to the axial direction. The amount of solute in the solvent is considered negligible, resulting in the fluid phase being described as pseudo-homogeneous, and its properties are assumed to be the same as the solvent. The mass balance equation for the fluid phase includes convection, diffusion, and kinetic terms.

$$\frac{\partial c_f(t,z)}{\partial t}+\frac{1}{\phi(z)}\frac{\partial\left(c_f(t,z)u\right)}{\partial z}=\frac{1-\phi(z)}{\phi(z)}r_e(t,z)+\frac{1}{\phi(z)}\frac{\partial}{\partial z}\left(D_e^M\frac{\partial c_f(t,z)}{\partial z}\right) \tag{9}$$

$c_f(t,z)$ represents the concentration of solute in the fluid phase, , $r_e(t,z)$ is a mass transfer kinetic term, and $D_e^M(T(t,z),P(t),F(t))$ is the axial mass diffusion coefficient.

2.3.3. Mass balance for the solid phase

The solid phase is considered to be stationary, with negligible convection and diffusion terms in the mass balance equation (Equation 10). Therefore, the only significant term in this equation is the kinetic term (as defined in Equation 11), which connects the solid and fluid phases. The extract

is represented by a single pseudo-component to simplify the analysis.

$$\frac{\partial c_s(t,z)}{\partial t} = \underbrace{r_e(t,z)}_{\text{Kinetics}} \tag{10}$$

2.3.4. Kinetic term

The kinetic term in this study is based on the two-film theory proposed by Reverchon [4], and the mass transfer kinetic is given by Equation 11. This equation takes into account the overall diffusion coefficient and the concentration gradient, which acts as the driving force for the process.

As the solvent flows through the bed, CO_2 molecules diffuse into the pores and adsorb on the particle surface to form an external fluid film around the solid particles due to the solvent-solid matrix interactions. The effect of Knudsen diffusion is negligible in this process, as the mean free path of the molecule is much smaller than the pore diameter. The dissolved solute diffuses from the particle's core through the solid-fluid interface, the pore, and the film into the bulk. Figure 4 illustrates the mass transfer mechanism, where the mean solute concentration in the solid phase is denoted as c_s and the equilibrium concentrations at the solid-fluid interface are denoted as c_s^* and c_p^*, respectively, for solid and fluid phases. The concentration of the solutes in the fluid phase in the center of the pore is denoted as c_p. As the solute diffuses through the pore, its concentration changes and reaches c_{pf} at the opening of the pore. The solute then diffuses through the film around the particle and reaches a concentration in bulk c_f. The two-film theory describes the solid-fluid interface inside the pore. The overall mass transfer coefficient can be determined if the relationship between the solute concentration in one phase and its equilibrium concentration is known.

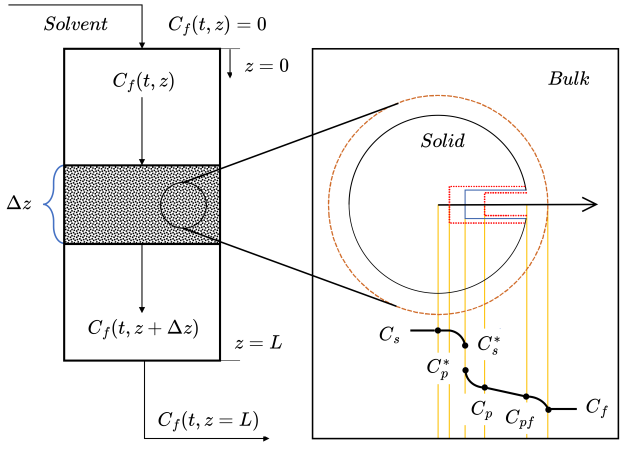

Figure 4: The extraction mechanism

Bulley et al. [15] suggests a process where the driving force for extraction is given by the difference between the concentration of the solute in bulk, c_f, and in the center of the pore, c_p^*. The concentration c_p^* is in equilibrium with c_s according to an equilibrium relationship. The rate of extraction is thus $r_e\left(c_f - c_p^*(c_s)\right)$.

On the other hand, Reverchon [4] proposes a driving force given by the difference between c_s and c_p^*. c_p^* is determined by an equilibrium relationship with c_f and the extraction rate is $r_e\left(c_s - c_p^*(c_f)\right)$ or more precisely

$$r_e(t,z) = \frac{D_i(T(t,z),P(t))}{\mu l^2}\left(c_s(t,z) - c_P^*(t,z)\right) \tag{11}$$

where μ is sphericity, l a characteristic dimension of particles and can be defined as $l = r/3$, r is the mean particle radius, ρ_s is the solid density, $D_i(T(t,z))$ corresponds to the overall diffusion coefficient and $c_P^*(t,z)$ is a concentration at the solid-fluid interface (which according to the internal resistance model is supposed to be at equilibrium with the fluid phase).

According to Bulley et al. [15], a linear equilibrium relationship (equation 12) can be used to find an equilibrium concentration of the solute in the fluid phase $c_f^*(t,z)$ is based on the concentration of the solute in the solid phase $c_s(t,z)$

$$c(t,z) = k_p(T(t,z),P(t))q^*(t,z) \tag{12}$$

The volumetric partition coefficient $k_p(T(t,z),P(t))$ behaves as an equilibrium constant between the solute concentration in one phase and the corresponding equilibrium concentration at the solid-fluid interphase. According to Spiro and Kandiah [16], the term $k_p(T(t,z),P(t))$ can be expressed as the function of mass partition factor $k_m(T(t,z))$.

$$k_m(T(t,z)) = \frac{k_p(T(t,z),P(t))\rho_s}{\rho(T(t,z),P(t))} \tag{13}$$

Equation 14 represents of the kinetic term according to Reverchon [4]

$$r_e(t,z) = -\frac{D_i(T(t,z),P(t))}{\mu l^2}\left(c_s(t,z) - \frac{\rho_s}{k_m(T(t,z))\rho_f(T(t,z),P(t))}c_f(t,z)\right) \tag{14}$$

2.3.5. Uneven distribution of the solute in the solid phase

Following the idea of the Broken-and-Intact Cell (BIC) model presented by Sovova [17], the internal diffusion coefficient D_i is consider to be a product of the reference value of D_i^R and the exponential decay function γ, as given by Equation 15.

$$D_i = D_i^R\gamma(c_s(t,z)) = D_i^R\exp\left(\Upsilon\left(1 - \frac{c_s(t,z)}{c_{s0}}\right)\right) \tag{15}$$

where the Υ describe the curvature of the decay function. The final form of the extraction kinetic Equation is given by Equation 16.

$$r_e(t,z) = -\frac{D_i^R(T(t,z),P(t))\gamma(c_s(t,z))}{\mu l^2}\left(c_s(t,z) - \frac{\rho_s}{k_m(T(t,z))\rho(T(t,z),P(t))}c_f(t,z)\right) \tag{16}$$

Such a formulation limits the availability of the solute in the solid phase. Similarly to the BIC model, if solute

is assumed to be contained in the cells, a part of which is open because the cell walls were broken by grinding, and the rest remains intact. The diffusion of the solute from a particle's core takes more time compared to the diffusion of the solute located close to the outer surface. Considering that the internal diffusion coefficient decay as the concentration of the solute in the solid decrease. As the value of the c_s decrease over time, the exponential term approach unity and $\lim_{c_s \to 0} D_i = D_i^R$. D_i^R can be interpreted as the internal diffusion coefficient at vanishing gradient.

Alternatively, the decay function γ can be consider with respect to the Shrinking Core model presented by Goto et al. [18], where the particle radius change as the amount of solute in the solid phase decrease. As the particle size decrease due to dissolution, the diffusion path increase which makes the diffusion slower and reduce the value of a diffusion coefficient. The same analogy can be apply to the Equation 15 to explain the change of the diffusion coefficient.

2.3.6. Heat balance

The heat governing equation describe the evolution of the energy in the system and it is given by 17. The derivation of the heat equation can be found in Appendix **??**.

$$\frac{\partial \left(\rho_f(T(t,z),P(t))e(t,z)A_f\right)}{\partial t} + \frac{\partial \left(\rho_f(T(t,z),P(t))A_f v e(t,z)\right)}{\partial z} = -P(t)\frac{\left(A_f v\right)}{\partial z} + \frac{\partial}{\partial z}\left(\frac{\partial T(t,z)}{\partial z}\right) \tag{17}$$

The departure function is a mathematical function that characterizes the deviation of a thermodynamic property (enthalpy, entropy, and internal energy) of a real substance from that of an ideal gas at the same temperature and pressure. The departure function is typically defined as the difference between the value of a thermodynamic property for a real fluid and the corresponding value for an ideal gas at the same temperature and pressure. They are typically computed by integrating a function that depends on the equation of state and its derivatives. Following Elliott [5] or Gmehling et al. [19], a real gas internal energy definition can be obtained from the departure functions, defined through Equation 18. More information on the departure functions can be found in Appendix **??**.

$$de(t,z) = C_v dT - \left[P(t) - T(t,z)\left(\frac{\partial P(t)}{\partial T(t,z)}\right)_{v_m(T(t,z),P(t))}\right] dv_m\left(T(t,z),P(t)\right) \tag{18}$$

where $e^{id}(t,z)$ is the internal energy of perfect gas.

Suppose a gas is considered to be perfectly caloric ($e(t,z) = C_v T(t,z)$), then the energy equation can be written explicitly in the form of temperature. The perfectly caloric gas can be seen as the special case of a real gas, where the second term of Equation 18 goes to zero and the heat capacity C_v is constant.

For real gases, it is complicated to write the heat balance in terms of temperature, but it be can be used directly in the form of internal energy, as it is given by Equation 3. In such a case, the temperature needs to be recovered from the internal energy. A relation for the internal energy can be obtained from an equation of state. For Peng-Robinson, such a relation is given by Equation 19 as presented by Elliott [5].

$$\frac{e(t,z) - e^{id}(t,z)}{RT(t,z)} = -\frac{A\left(T(t,z),P(t)\right)}{B\left(T(t,z),P(t)\right)\sqrt{8}}\frac{\kappa\sqrt{T_r}}{\sqrt{\alpha}}\ln\left[\frac{Z\left(T(t,z),P(t)\right) + \left(1+\sqrt{2}\right)B\left(T(t,z),P(t)\right)}{Z\left(T(t,z),P(t)\right) + \left(1-\sqrt{2}\right)B\left(T(t,z),P(t)\right)}\right] \tag{19}$$

To solve Equation 19, temperature, pressure, and density values need to be known. If an equation of state is introduced, then only two out of three variables need to be obtained as the third one can be calculated; this can be represented as follow

$$e(t,z) = e(T(t,z),P(t),\rho_f(T(t,z),P(t))) = e(T(t,z),P(t),\rho_f(T(t,z),P(t))) \tag{20}$$

If the value of internal energy $e(t,z)$ is known from the time evolution of the energy Equation 3, and pressure is known from measurement, then the temperature can be reconstructed. A roootfinder can be used to find a value of temperature, which minimizes the difference between the value of internal energy coming from the time evolution (Equation 17) and the output from Equation 19. Such a procedure allow to find local temperature along spatial direction z and needs to be repeated every time-step.

Another way to express the energy equation is to introduce enthalpy $h(t,z) = e(t,z) + P(t)/\rho_f(T(t,z),P(t))$. By introducing the definition of enthalpy, the energy equation becomes

$$\frac{\partial \left(\rho_f(T(t,z),P(t))h(t,z)A_f\right)}{\partial t} - \frac{\partial \left(P(t)A_f\right)}{\partial t} + \frac{\partial \left(\rho_f(T(t,z),P(t))h(t,z)A_f v\right)}{\partial z} - \frac{\partial}{\partial z}\left(k\frac{\partial T(t,z)}{\partial z}\right) \tag{21}$$

The main advantage of this formulation is the presence of term $\partial P(t)/\partial t$, which allows it to directly affect the system through the change of thermodynamic pressure (which is a control variable). The enthalpy is related to the pressure and temperature through the following equation:

$$h(t,z) = h(T(t,z),P(t),\rho_f(T(t,z),P(t))) = h(T(t,z),P(t),\rho_f(T(t,z),P(t))) \tag{22}$$

If the value of enthalpy is known from the time evolution and pressure can be measured, then the Equation 22 can be solved for the temperature to recover the temperature profile. For the Peng-Robinson EoS, the enthalpy can be defined by Equation 23. More details can be found in Appendix **??** or given by Gmehling et al. [19].

$$h(t,z) - h(t,z)^{id} = RT(t,z)\left[T_r(Z\left(T(t,z),P(t)\right) - 1) - 2.078(1+\kappa)\sqrt{\alpha\left(T(t,z)\right)}\ln\left(\frac{Z\left(T(t,z),P(t)\right) + \left(1+\sqrt{2}\right)B\left(T(t,z),P(t)\right)}{Z\left(T(t,z),P(t)\right) + \left(1-\sqrt{2}\right)B\left(T(t,z),P(t)\right)}\right)\right] \tag{23}$$

The Equation 23 requires an reference sate, which in this case is assumed to be $T_{ref} = 298.15\ [K]$ and $P_{ref} = 1.01325\ [bar]$.

As discussed by Gmehling et al. [19], the influence of the intermolecular forces on the enthalpy is needs to taken into account in high pressures systems. In most cases, these forces are attractive, so additional energy is necessary to move the molecules away from each other, that is, to lower the density. If this energy is not added, the substance cools down when it is expanded.

2.3.7. Pressure term

The pressure term in the energy equation, given by Equation 21, describes the change of the thermodynamic pressure with respect to time. As explained in Chapters 2.2, at Low-Mach number conditions, the thermodynamic pressure is nearly constant in space due to the small pressure wave propagation that occurs at the speed of sound. Under such conditions, the term $\partial P/\partial t$ can be approximated by an ordinary differential equation, which describes the instantaneous change of pressure in the system. The pressure (P) in the system is considered a state variable, while the pressure in the new time-step (P_{in}) is considered a control variable.

$$\frac{\partial P(t)}{\partial t} \approx \frac{P(t) - P_{in}(t)}{\Delta t} \tag{24}$$

Such a simplified equation takes into account the pressure change in the energy balance, but the dynamics are simplified and do not consider the effects of pressure losses. In a real system, the dynamics of pressure change would depend on a pump used in an extraction system, as well as a back-pressure regulator used to control an outlet valve.

2.3.8. Extraction yield

The efficiency of the process (the yield) is calculated according to Equation 25 as presented by Sovova et al. [20]. The measurement equation evaluate the mass of solute at the outlet of the extraction unit and sums it. The integral form of the measurement equation (25) can be transformed into the differential form (26) and augmented with the process model.

$$y(t) = \int_{t_0}^{t_f} \frac{F(t)}{\rho_f(T(t,z),P(t))} c_f(t,z)\Big|_{z=L} dt \tag{25}$$

$$\frac{dy(t)}{dt} = \frac{F(t)}{\rho_f(T(t,z),P(t))} c_f(t,z)\Big|_{z=L} \tag{26}$$

2.3.9. Initial and boundary conditions

It is assumed that the solvent is free of solute at the entrance of the extractor and that all the solid particles have the same initial solute content c_{s0}. Every SFE system needs some time to reach the desired operating conditions but the solute diffuses from solid phase to the fluid phase already at the preparation stage. For instance, a pump introduce more fluid to the extractor to increase the pressure, which makes the fluid present already in that vessel to moves internally hence the solute in the fluid phase is non-uniformly distributed. Some conclusions can be drawn from the analysis of the initial part of each yield curve obtained from the laboratory (Figure **??**). It can be noticed that each curve at the beginning has a non-linear curvature. A quadratic function could approximate the initial part of each extraction curve. A function that, after integration, gives a quadratic-like result is a straight line. Based on that observation, the solute concentration in the fluid phase is assumed to be linearly distributed. The solute concentration is assumed to be zero at the outlet and reach the maximum at the beginning of the fixed bed. The details on the calculation are given in Appendix **??**. The linear distribution $H(z)$ can be defined if the total mass of solute m_{total} and initial mass ratio between solid and fluid phases τ are known. Moreover, it is considered that the initial temperature of the extractor in every place is the same and described by h_0. Therefore, the initial conditions employed in the simulation are:

$$c_f(t=0,z) = H(z) \quad c_s(t=0,z) = c_{s0} \quad h(t=0,z) = h_0$$

2.3.10. State-space representation

The process model can be written in a general form:

$$\begin{bmatrix} \frac{\partial c_f(t,z)}{\partial t} \\ \frac{\partial c_s(t,z)}{\partial t} \\ \frac{\partial h(t,z)}{\partial t} \\ \frac{\partial P(t,z)}{\partial t} \\ \frac{\partial y(t)}{\partial t} \end{bmatrix} = \begin{bmatrix} \bar{\phi}_1\left(c_f(t,z), c_s(t,z), h(t,z); \Theta\right) \\ \bar{\phi}_2\left(c_f(t,z), c_s(t,z), h(t,z); \Theta\right) \\ \bar{\phi}_3\left(c_f(t,z), c_s(t,z), h(t,z); \Theta\right) \\ \bar{\phi}_4\left(c_f(t,z), c_s(t,z), h(t,z); \Theta\right) \\ \bar{\phi}_5\left(c_f(t,z), c_s(t,z), h(t,z); \Theta\right) \end{bmatrix} = \bar{\phi}(t,z;\Theta) = \frac{\partial \chi(t,z)}{\partial t} \tag{27}$$

where Θ is a paramter space, $\bar{\phi}$ is a set of functions that correspond to state equations of the model, and χ is the state-space model.

Function $\bar{\phi}$ are transformed to a corresponding set of N_z discretized equations denoted as G. The state-space model $\chi(t,z)$ after the discretization is represented by $\dot{x}(t)$.

$$\dot{x}(t) = \frac{dx(t)}{dt} = \begin{bmatrix} \frac{dc_{f,1}(t)}{dt} \\ \vdots \\ \frac{dc_{f,N_z}(t)}{dt} \\ \hline \frac{dc_{s,1}(t)}{dt} \\ \vdots \\ \frac{dc_{s,N_z}(t)}{dt} \\ \hline \frac{dh_1(t)}{dt} \\ \vdots \\ \frac{dh_{N_z}(t)}{dt} \\ \hline \frac{dP(t)}{dt} \\ \hline \frac{dy(t)}{dt} \end{bmatrix} = \underbrace{\begin{bmatrix} G_1\left(c_f(t), c_s(t), h(t); \Theta\right) \\ \vdots \\ G_{N_z}\left(c_f(t), c_s(t), h(t); \Theta\right) \\ \hline G_{N_z+1}\left(c_f(t), c_s(t), h(t); \Theta\right) \\ \vdots \\ G_{2N_z}\left(c(t), c_s(t), h(t); \Theta\right) \\ \hline G_{2N_z+1}\left(c_f(t), c_s(t), h(t); \Theta\right) \\ \vdots \\ G_{3N_z}\left(c_f(t), c_s(t), h(t); \Theta\right) \\ \hline G_{3N_z+1}\left(c_f(t), c_s(t), h(t); \Theta\right) \\ \hline G_{3N_z+2}\left(c_f(t), c_s(t), h(t); \Theta\right) \end{bmatrix}}_{G(x(t);\Theta)}$$

where $x \in \mathbb{R}^{N_x=3N_z}$ and $\Theta \in \mathbb{R}^{N_\Theta=N_\theta+N_u}$, N_θ is the number of model parameters, N_u is the number of control variables.

In a state-space sense, the state variables of the system are the local concentrations of solute in the fluid and solid phases ($c_f(t,z)$ and $c_s(t,z)$, respectively), and the local enthalpy of the pseudo-homogeneous phase ($h(t,z)$). The controllable input variables are the mass flow-rate and temperature of the solvent in the feed and the pressure in the extractor. Additionally, the pressure change is augumented with the state-space and denoted as $P(t)$. The system state-space is extended by assuming that extraction yield can be modelled as a function of a known initial mass of solute in the solid phase and it can be measured after the separator ($Y(t)$). The system is controllable by manipulating the flow-rate and temperature (enthalpy) of CO_2 in the feed, and the pressure in the extractor.

2.3.11. Discretization methods

The method of lines is used to transform the process model equations into a set of ODEs denoted as $G(x(t);\Theta)$. The partial derivatives in z-direction are computed using a first-order and second-order finite difference approximation. The backward finite difference is used to approximate the first-order derivative, while the central difference scheme is used to approximate the second-order derivative. The length of the fixed bed is divided into N_z equally distributed points in z-direction.

As presented in Appendix **??**, all the governing can be written in the integral form using the Divergence Theorem. The integral equation states that the change rate of the integral of any quantity over an arbitrary control volume is given by the flux through the boundary of the control volume, with being the outer surface normal through the boundary. That quantity is neither produced nor consumed inside of the control volume and is hence conserved. For a derivative to be conservative, it must form a telescoping series. In other words, after the addition of all terms coming from the discretization over a grid, only the boundary terms should remain and the artificial interior points should cancel out. To ensure the mass conservation, the discretization is applied on the conservative form of the process model.

2.4. Sensitivity Analysis

Local derivative-based methods involve taking the partial derivative of the output with respect to an input parameter. This set of derivatives is known as sensitivity equations, and it is solved simultaneously with the process model. The purpose of the sensitivity analysis is to investigate how responsive the solution is for the perturbation of the parameter p. According to Dickinson and Gelinas [21], the sensitivity analysis can be used to determine the influence of the uncertainty on the solution of the original system. Another purpose is to distinguish sensitive parameters from insensitive ones, which might be helpful for model reduction. Finally, from a control engineering point of view, the sensitivity analysis allows to sort the control variables with respect to the level of effort required to change the model's output.

As presented in the work of Maly and Petzold [22], the sensitivity analysis equations($\dot{Z}$) are developed by taking the total derivative of the original system $F(x(t);p)$ with respect to p.

$$Z(x(t);p) = \frac{\partial x(t)}{\partial p} \tag{28}$$

As the process model depends on time t, parameters p and initial conditions, each parameter's sensitivity also depend on time t. Therefore, the new system of equations can be obtained by taking derivatives with respect to time t and applying the chain rule.

$$\dot{Z}(x(t);p) = \frac{dZ(x(t);p)}{dt} = \frac{\partial}{\partial t}\left(\frac{\partial x(t)}{\partial p}\right) = \frac{\partial}{\partial p}\left(\frac{\partial x(t)}{\partial t}\right) = \frac{dF(x(t);p)}{dp} \tag{29}$$

By applying the definition of the total derivative to the equation 29, the sensitivity equation can be obtained.

$$\frac{dF(x(t);p)}{dp} = \underbrace{\frac{\partial F(x(t);p)}{\partial x(t)}}_{J_x(x(t);p)}\underbrace{\frac{\partial x(t)}{\partial p}}_{S(x(t);p)} + \underbrace{\frac{\partial F(x(t);p)}{\partial p}}_{J_p(x(t);p)} \tag{30}$$

The sensitivity equation 30 is solved simultaneously with the original system. This equation is made of three terms: jacobian $J_x(x(t);p)$, sensitivity matrix $S(x(t);p)$ and jacobian $J_p(x(t);p)$. The jacobian $J_x(x(t);p)$ represents the matrix of equations of size $N_x \times N_x$, where each equation $J_x(n_x,n_x)$ is the derivative of process model equations $F_{n_x}(x(t);p)$ with respect to the state variable x_{n_p}.

$$J_x(x(t);p) = \begin{pmatrix} \frac{\partial F_1(x(t);p)}{\partial x_1(t)} & \frac{\partial F_1(x(t);p)}{\partial x_2(t)} & \cdots & \frac{\partial F_1(x(t);p)}{\partial x_{N_x}(t)} \\ \frac{\partial F_2(x(t);p)}{\partial x_1(t)} & \frac{\partial F_2(x(t);p)}{\partial x_2(t)} & \cdots & \frac{\partial F_2(x(t);p)}{\partial x_{N_x}(t)} \\ \vdots & \vdots & \ddots & \vdots \\ \frac{\partial F_{N_x}(x(t);p)}{\partial x_1(t)} & \frac{\partial F_{N_x}(x(t);p)}{\partial x_2(t)} & \cdots & \frac{\partial F_{N_x}(x(t);p)}{\partial x_{N_x}(t)} \end{pmatrix} \tag{31}$$

The sensitivity matrix $S(x(t);p)$ represents the matrix of equations of size $N_x \times N_p$, where each equation $S(n_x,n_p)$ is the derivative of the state variable x_{n_x} with respect to the parameter p_{n_p}.

$$S(x(t);p) = \begin{pmatrix} \frac{dx_1(t)}{dp_1} & \frac{dx_1(t)}{dp_2} & \cdots & \frac{dx_1(t)}{dp_{N_p}} \\ \frac{dx_2(t)}{dp_1} & \frac{dx_2(t)}{dp_2} & \cdots & \frac{dx_2(t)}{dp_{N_p}} \\ \vdots & \vdots & \ddots & \vdots \\ \frac{dx_{N_x}(t)}{dp_1} & \frac{dx_{N_x}(t)}{dp_2} & \cdots & \frac{dx_{N_x}(t)}{dp_{N_p}} \end{pmatrix} \tag{32}$$

The jacobian $J_p(x(t);p)$ represents the matrix of equations of size $N_x \times N_p$, where each equation $J_p(n_x,n_p)$ is the direct derivative of the process model equation F_{n_x} with respect to the parameter p_{n_p}.

$$J_p(x(t);p) = \begin{pmatrix} \frac{\partial F_1(x(t);p)}{\partial p_1} & \frac{\partial F_1(x(t);p)}{\partial p_2} & \cdots & \frac{\partial F_1(x(t);p)}{\partial p_{N_p}} \\ \frac{\partial F_2(x(t);p)}{\partial p_1} & \frac{\partial F_2(x(t);p)}{\partial p_2} & \cdots & \frac{\partial F_2(x(t);p)}{\partial p_{N_p}} \\ \vdots & \vdots & \ddots & \vdots \\ \frac{\partial F_{N_x}(x(t);p)}{\partial p_1} & \frac{\partial F_{N_x}(x(t);p)}{\partial p_2} & \cdots & \frac{\partial F_{N_x}(x(t);p)}{\partial p_{N_p}} \end{pmatrix} \tag{33}$$

The combined system containing the original set of equations $F(x(t);p)$ and sensitivity equations can be formulated as $\mathbf{F}(x(t);p)$. The size of $\mathbf{F}(x(t);p)$ is equal to $N_s = N_x(N_p+1)$.

$$\mathbf{F}(x(t);p) = \begin{bmatrix} F(x(t);p) \\ J_x(x(t);p)S(x(t);p) + J_p(x(t);p) \end{bmatrix} \tag{34}$$

The initial conditions are described as

$$\mathbf{F}\left(x(t_0);p\right) = \left[x(t_0), \quad \frac{\mathrm{d}x(t_0)}{dp_1}, \quad \cdots, \quad \frac{dx(t_0)}{dp_{N_p}} \right]^T \tag{35}$$

In a similar way, the sensitivity analysis of the output function can be performed with respect to parameters p. The output function $g(x(t))$ returns $y(t)$. By taking a total derivative of $y(t)$ with respect to p, the new sensitivity equation can be found.

$$\frac{dy(t)}{dp} = \frac{dg(x(t))}{dp} = \frac{\partial g(x(t))}{\partial x(t)}\frac{\partial x(t)}{\partial p} + \frac{\partial g(x(t))}{\partial p} \tag{36}$$

3. Results

The sensitivity equations were solved simultaneously with the original process model. This work investigates the influence of inlet temperature, pressure, and mass flow rate on the state space and the extraction yield. The process model and parameters have been discussed in article 1. The process model was calibrated on set of experiments obtained at different operating conditions, 40°C - 50°C and 200 bar - 300 bar. The sensitivity analysis has been performed under the assumption that the system operates are 45°C, 250 bar, 0.4 l/min. The simulation was performed with the time step of 0.01 [min] and 400 equally distributed points in the spatial direction.

3.1. Flow-rate

The increase in the mass-flow rate affects the whole system simultaneously in the spatial direction. The change in mass flow-rate makes the fluid move faster and does not directly affect the thermodynamic state of the fluid. As a result, Figure 5 shows no change in pressure during the simulation.

A flow rate change is defined by the spatial derivative $\frac{\partial(\rho_f h A_f v)}{\partial z}$. The consequence of Equation **??** is the instantaneous change of the velocity field in the system, which means that the spatial derivative equals zero. It's important to note that h represents enthalpy but not total enthalpy, thus excluding kinetic energy contribution. As a consequence of our modelling assumptions, changes in h and ρ_f only occur in response to direct change in pressure or temperature. As the result, Figure 6 demonstrates no significant deviation.

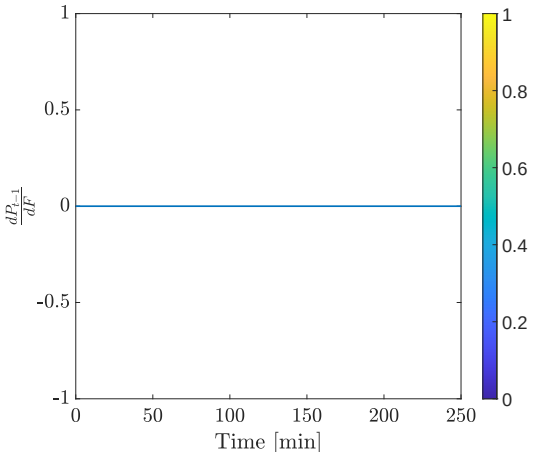

Figure 5: The effect of F change on P

The flow rate change affects the fluid inside the system, but appropriate boundary conditions must be set. When utilizing Dirichlet boundary conditions, it's crucial to be aware of potential numerical discrepancies stemming from the differing methods used to compute them. The system's enthalpy is determined through the time evolution of governing equations, while the inlet's enthalpy depends on the inlet temperature and pressure. A minor numerical mismatch between these values may manifest as an enthalpy difference propagating along the spatial domain. To ensure consistency between the fluid at the inlet and inside the computational domain, this analysis employs Neumann boundary conditions.

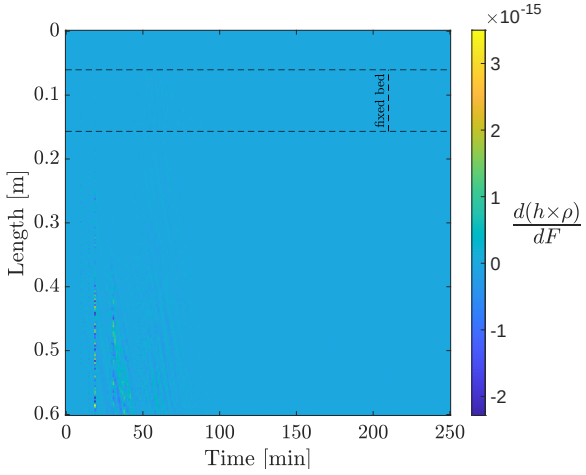

Figure 6: The effect of F change on $\rho \times h$

An increase in the mass flow rate impacts the concentration gradient and the extraction kinetics as presented in Figure 7 . At the beginning of the extraction process, changes in the flow rate have a minimal effect on the extraction process, as showed by sensitivities that are close to zero. This is due to the dominance of the high concentration gradient, which leads the extraction kinetic. As time progresses, the

increase in the mass flow rate have greater influence on the extraction kinetics, causing the sensitivities to decrease towards their minimum values. Negative sensitivities indicate a faster extraction rate. Over time, the amount of solute in the solid phase decreases, and eventually, the extraction kinetic becomes limited by the concentration gradient. This behavior is represented in the sensitivities, which asymptotically approach zero. The asymptotic movement of sensitivities can be explained by the fact that an increase in the flow rate does not impact the extraction process when all the solute has been removed from the solid phase.

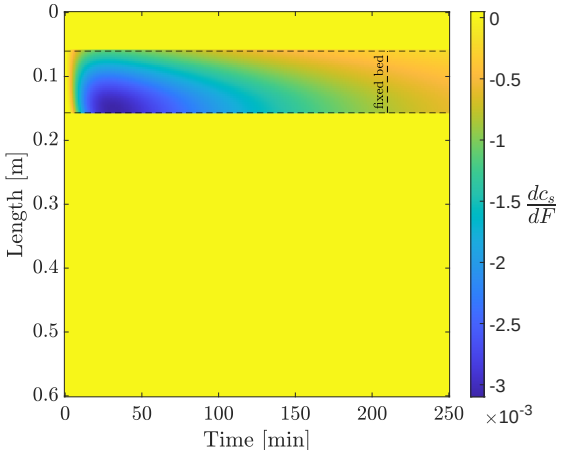

Figure 7: The effect of F change on C_s

Figure 8 illustrates how the concentration of solute in the fluid phase responds to an increase in the flow rate. Initially, sensitivities are close to zero, indicating a minimal system response. The growth in flow rate affects $C_f(z,t)$ by increasing the velocity, consequently elevating the concentration gradient. As a result, positive sensitivities emerge within the system, forming a front that progresses in the direction of flow. The positive front indicates that the larger amount of solute moves faster across the system, which leads to faster decrease of the total amount of solute in both phases. This reduced amount of solute in the solid phase restricts the extraction rate due to a diminishment of the concentration gradient. This limitation leads to the formation of a front composed of negative sensitivities, which advances through the extractor. The negative front indicates that the solute concentration in the fluid phase becomes lower than before the flow rate increment. Eventually, the negative sensitivities asymptotically approach zero.

Figure 9 illustrates how the increase in flow rate affects the extraction yield. Initially, the sensitivity curve remains flat. This occurs because the fixed bed doesn't occupy the entire volume of the extractor, requiring some time for the fluid to flow through the empty portion of the extractor to reach its outlet. It's only when the solute in the fluid phase reaches the extractor's outlet that we can measure and observe the system response. At this point, dy/dF begins to increase. The positive sensitivity value indicates an improvement in process efficiency, resulting in an increased yield.

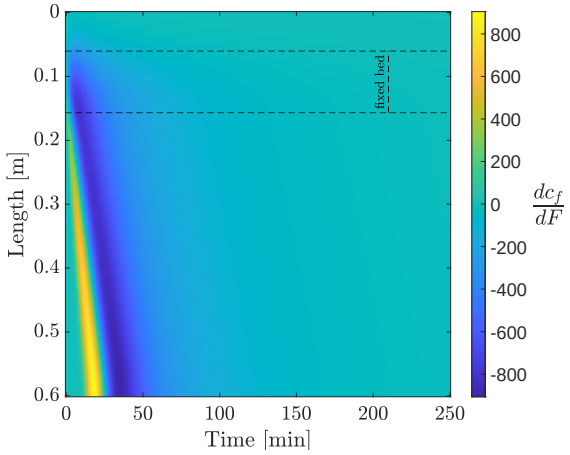

Figure 8: The effect of F change on C_f

As time progresses, the sensitivity reaches its maximum and then diminishes due to a decreasing concentration gradient. Eventually, dy/dF asymptotically approaches zero. This happens because the amount of solute in the fluid phase becomes a limiting factor in the extraction process, and the increase in flow rate has a reduced impact on the extraction yield. The simulation time was extended to demonstrate the convergence of dy/dF toward zero.

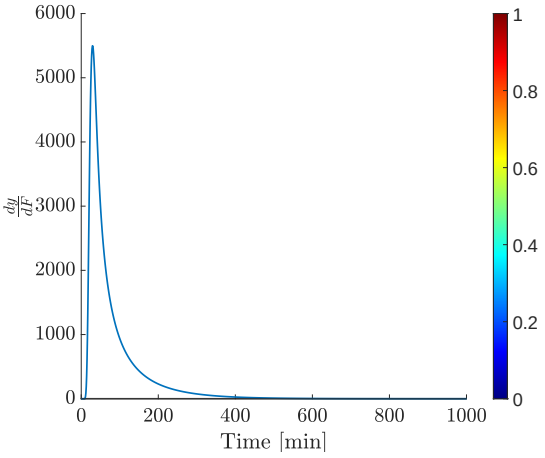

Figure 9: The effect of F change on $y(t)$

3.2. Pressure

As discussed in Chapter 2.2, a small pressure wave propagates at the speed of sound relative to the flow. If the flow velocity is relatively low, all pressure changes are hydrodynamic (resulting from velocity motion) rather than thermodynamic. The Low Mach-number assumption enables instant pressure propagation throughout the system. This assumption allows to consider a single pressure value for the entire system, as all changes occur simultaneously within the machine. Figure 10 illustrates a step function representing the pressure change in the system.

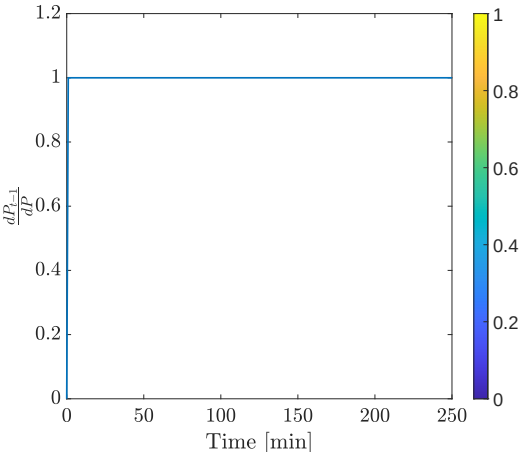

Figure 10: The effect of P change on P in the system

As a result of the Low Mach-number assumption and the pressure deviation, temperature and density change simultaneously along the system. According to Equation 21, the pressure change directly affects the quantity $h \times \rho_f$ through $\partial(P(t)A_f)/\partial t$, leading to the step change presented in Figure 11. Depending on the configuration of the system, two cases are possible. Since the total energy in the extractor has changed, there may be a difference between the fluid inside the equipment and the boundary conditions at the inlet. If Dirichlet boundary conditions are applied, the inlet temperature is maintained at the predefined value and may differ from the temperature in the extractor. In such a case, the temperature difference will cause the heat front to propagate through the system. Alternatively, Neumann boundary conditions can be applied to ensure that the temperature inside the extractor matches that at its inlet. In this work, the second approach was chosen to simplify the discussion.

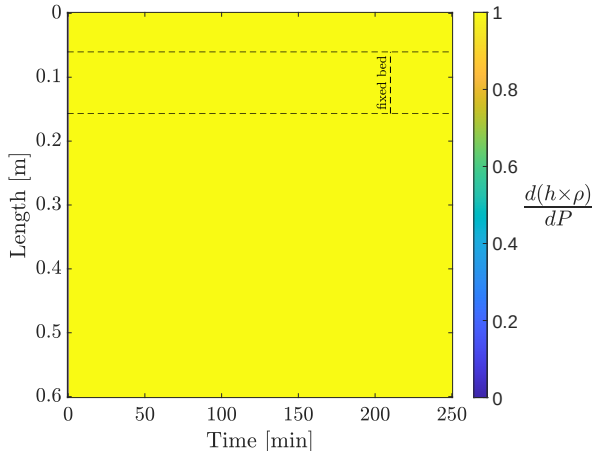

Figure 11: The effect of P change on $(h \times \rho_f)$ in the system

The pressure change affects the mass transfer in two ways. As given in Chapter 2.3.1, the velocity is inversely proportional to the density; hence, the higher density of the fluid leads to a lower velocity and larger residence time. The second way is given by the relationships, which connect the pressure and the extraction kinetic term. As presented in article 1, the D_i^R increases with the fluid density, which leads to a higher extraction rate. The cumulative effect of the pressure change can be observed in Figure 12. The sensitivity plot shows a uniform decay of sensitivities along the fixed bed. The negative values of sensitivities suggest a faster extraction rate. No matter the location of the sensitivity in the bed, the general behaviour stays the same. Every sensitivity starts with zero and decreases to a minimum value. After the extremum, the sensitivities asymptotically increase to zero.

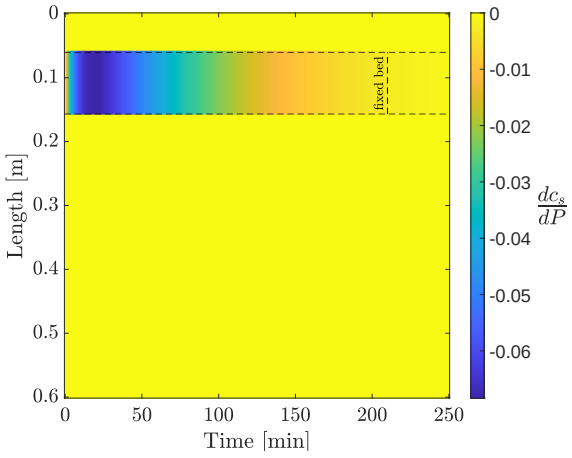

Figure 12: The effect of P change on C_s

The corresponding response of the pressure change on the solute concentration in the fluid phase is presented in Figure 13. As discussed earlier, the pressure change directly influences the extraction kinetics. Figure 12 is characterized by negative sensitivities, suggesting a higher extraction rate due to the pressure change. Consequently, an increase in solute concentration in the fluid phase is expected. This increase in solute concentration in the fluid phase is visible in Figure 13 as positive sensitivities, forming a front that moves along the extractor. As the extraction process accelerates, more solute enters the fluid phase, explaining the "hot spot" in the Figure. Subsequently, the solute flows through the system where there are no solid particles, and the diffusion effect becomes noticeable. Following the positive sensitivities, a small front of negative sensitivities can be observed. Due to the higher extraction rate, more solute has been extracted at the beginning of the extraction process, resulting in less solute available for extraction later. This effect is reflected in Figure 13 as negative sensitivities. Eventually, the negative sensitivities approach zero.

The impact of pressure increase on extraction yield is depicted in Figure 14. The initial flat curve reflects a system delay, caused by the empty space within the extractor that the solvent with solute must traverse to reach the outlet. Next, a positive sensitivity starts to rise, which indicates an increase in yield. dy/dP reaches its maximum and then declines due

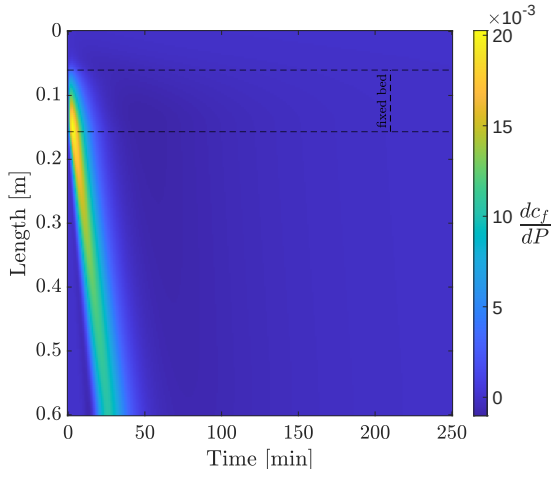

Figure 13: The effect of P change on C_f

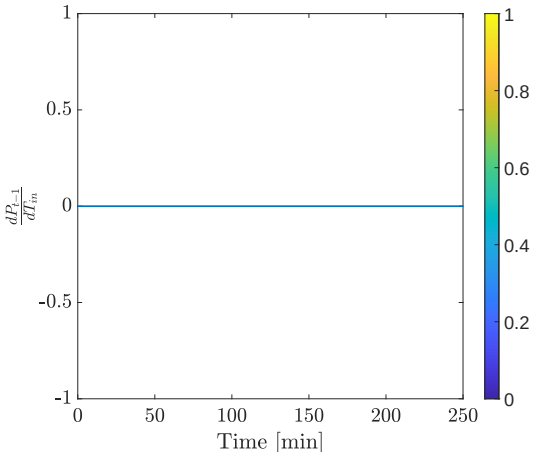

Figure 15: The effect of T_{in} change on P in the system

to a lower amount of solute remaining in the solid phase compared to the initial pressure conditions. This sensitivity eventually dips into negative values, hits a minimum point, and ultimately converges to zero. The simulation duration was extended to demonstrate the convergence of dy/dP towards zero.

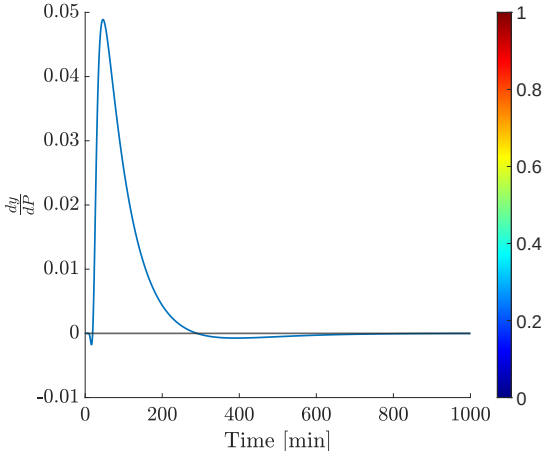

Figure 14: The effect of P change on $y(t)$

are predefined (Dirichlet boundary conditions) and consistent with those inside the system. The inlet value of $(h{\times}\rho_f)$ is calculated based on the provided inlet temperature and given pressure. Any deviation in T_{in} affects $(h \times \rho_f)$ at the inlet, which subsequently propagates according to the governing equations.

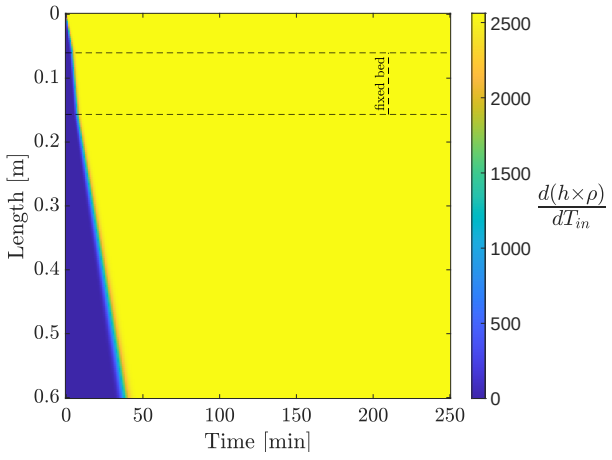

Figure 16: The effect of T_{in} change on $(h \times \rho_f)$ in the system

3.3. Inlet temperature

The impact of the inlet temperature on supercritical extraction differs from the two cases presented earlier because the disturbance does not instantaneously affect the entire system; instead, it propagates through the system. As the fluid with the modified temperature flows along the system, it gradually influences the mass transfer parameters. One important assumption is that the inlet temperature does not affect the pressure, and as a result, a horizontal line is present in Figure 15.

The propagation of the heat front is presented in Figure 16. Initially, the system was uniformly set to the same temperature. The temperatures at the inlet and outlet boundaries

Figure 17 illustrates how the change in inlet temperature affects the concentration of solute in the solid phase. Initially, the sensitivities are zero along the fixed bed because the heat front requires time to propagate to the fixed bed. Since this propagation is not instantaneous, a non-uniform distribution of sensitivities along the fixed bed becomes evident. All the sensitivities gradually increase until they reach their respective maxima. As presented in article 1, the value of D_i^R decreases as density decreases. Therefore, it is expected to observe positive sensitivities in Figure 17, indicating a slower extraction rate. When the concentration gradient becomes the limiting factor, the sensitivities start to decrease to zero.

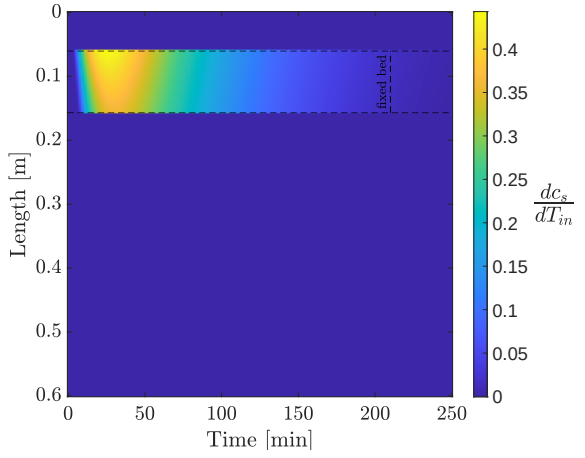

Figure 17: The effect of T_{in} change on C_s in the system

The influence of inlet temperature on solute concentration in the fluid phase is depicted in Figure 18. Initially, all the sensitivities remain at zero due to an idle period. When the fluid at the new temperature reaches the solid particles, it affects mass transfer, subsequently influencing the amount of solute in the fluid phase. In response to the slower extraction rate indicated by positive sensitivities in Figure 17, a section with negative sensitivities becomes visible in Figure 18. The effect of diffusion is observable in the section without the fixed bed, where the front composed of sensitivities becomes blurred. After reaching their minima, the sensitivities increase and attain positive values. This behavior can be explained by considering that the heat front slowed mass transfer, causing more solute to remain in the solid phase. This, in turn, leads to a higher concentration gradient in the later stages of extraction compared to the scenario without the inlet temperature deviation. The higher concentration gradient results in an increase in dc_f/dT_{in}.

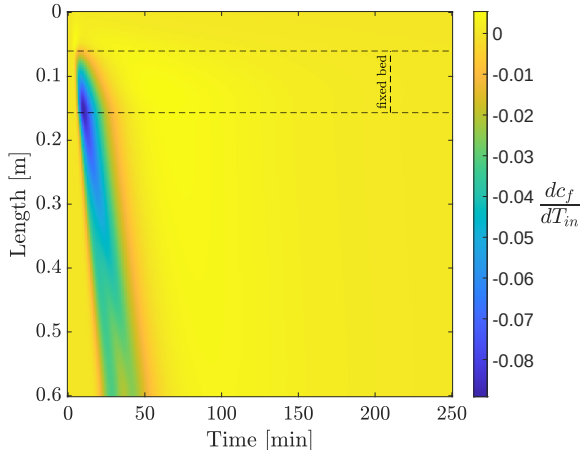

Figure 18: The effect of T_{in} change on C_f in the system

Figure 19 depicts how an increase in inlet temperature alters the extraction yield. Initially, the sensitivity curve remains flat. It is because the fixed bed doesn't occupy the entire volume of the extractor and the fluid requires some time to flow through the empty portion of the extractor to reach its outlet. It's only when the solute in the fluid phase reaches the extractor's outlet a system response can be observed. At this point, dy/dT_{in} begins to decrease, and the negative sensitivity value indicates a decrease in process efficiency. Over time, the sensitivity reaches its minimum and then increases due to a higher concentration gradient compared to the case without the disturbance. The sensitivity reaches a positive maximum and then declines again due to reduced extraction kinetics and a decreased concentration gradient. dy/dT_{in} becomes negative once more, eventually resulting in a flattening of the sensitivity curve. The flattening of the yield curve suggest that the mass transfer parameters limits the extraction rate and the residual solute in the solid phase become difficult to obtain.

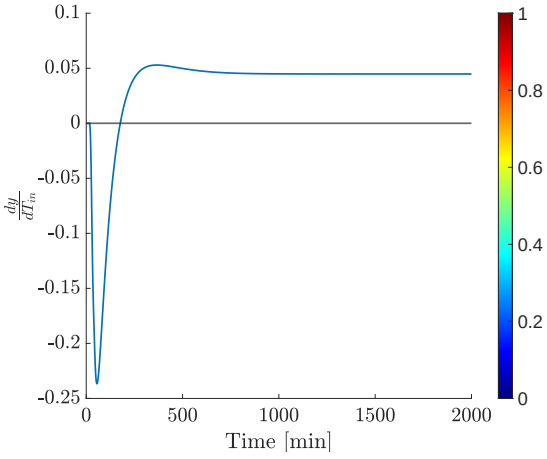

Figure 19: The effect of T_{in} change on $y(t)$ in the system

4. Conclusions

The sensitivity analysis is a tool to understand the parametric dependence of dynamic behavior and its suitability in inferring mechanisms of the dynamic behavior of the analyzed system. The mathematical formulation involves derivative-based local sensitivity analysis of the solution of an inverse problem with respect to perturbations of parameters. The local method is based only on considering all parameters as constants (those independent of time or location), and then the sensitivity coefficients are estimated by solving a variational system simultaneously with the original system. The sensitivity equations can be obtained in various ways, but in the case of this work, the automatic differentiation technique was implemented to obtain the sensitivity equations. By identifying which parameters are influential at each period of the simulation, local sensitivity analysis can yield valuable information for guiding the design of experiments, the process modeling, or the

model reduction. The local sensitivity analysis techniques consider the sensitivities at only a small region of parameter space, and the conclusions derived from such an analysis are limited to local conditions unless the discussed system is a linear system.

In this study, the local sensitivity analysis method was introduced to explore the dynamics of the supercritical extraction system, which consists of a set of partial differential equations. The sensitivity equations evaluate the influence of control variables such as flow rate, pressure, and inlet temperature on the state-space consisting of the concentration of the solute in solid and liquid phases, the fluid's enthalpy density, system pressure, and extraction yield. Every change in the control variables leads to a state-space change, eventually affecting the process performance. This information can be utilized to identify which control variables influence the extraction yield the most. The controls with high sensitivities on the extraction can be used to investigated to find optimal operating conditions from economic point of view.

References

[1] Nevena M. Hromis, Vera L. Lazic, Sinisa L. Markov, Zuzana G. Vastag, Senka Z. Popovic, Danijela Z. Suput, Natalija R. Dzinic, Aleksandra S. Velicanski, and Ljiljana M. Popovic. Optimization of chitosan biofilm properties by addition of caraway essential oil and beeswax. Journal of Food Engineering, 158:86–93, aug 2015. doi: 10.1016/j.jfoodeng.2015.01.001.

[2] Ernesto Reverchon, Giorgio Donsi, and Libero Sesti Osseo. Modeling of supercritical fluid extraction from herbaceous matrices. Industrial & Engineering Chemistry Research, 32(11):2721–2726, nov 1993. doi: 10.1021/ie00023a039.

[3] H. Sovova. Rate of the vegetable oil extraction with supercritical co2. modelling of extraction curves. Chemical Engineering Science, 49 (3):409–414, 1994. doi: 10.1016/0009-2509(94)87012-8.

[4] E. Reverchon. Mathematical modeling of supercritical extraction of sage oil. AIChE Journal, 42(6):1765–1771, jun 1996. doi: 10.1002/aic.690420627.

[5] J Elliott. Introductory chemical engineering thermodynamics. Prentice Hall, Upper Saddle River, NJ, 2011. ISBN 9780136068549.

[6] G. G. Simeoni, T. Bryk, F. A. Gorelli, M. Krisch, G. Ruocco, M. Santoro, and T. Scopigno. The widom line as the crossover between liquid-like and gas-like behaviour in supercritical fluids. Nature Physics, 6(7):503–507, jun 2010. doi: 10.1038/nphys1683.

[7] Daniel Banuti. The latent heat of supercritical fluids. Periodica Polytechnica Chemical Engineering, 63(2):270–275, jan 2019. doi: 10.3311/ppch.12871.

[8] W. Sheng, G. J. Chen, and H. C. Lu. Prediction of transport properties of dense gases and liquids by the peng-robinson (PR) equation of state. International Journal of Thermophysics, 10(1):133–144, jan 1989. doi: 10.1007/bf00500714.

[9] Sydney Chapman and T. G. Cowling. The Mathematical Theory of Non-uniform Gases. Cambridge University Press, 1991. ISBN 9780521408448.

[10] A. Fenghour, William A. Wakeham, and V. Vesovic. The viscosity of carbon dioxide. Journal of Physical and Chemical Reference Data, 27 (1):31–44, jan 1998. doi: 10.1063/1.556013.

[11] Arno Laesecke and Chris D. Muzny. Reference correlation for the viscosity of carbon dioxide. Journal of Physical and Chemical Reference Data, 46(1):013107, mar 2017. doi: 10.1063/1.4977429.

[12] M. L. Huber, E. A. Sykioti, M. J. Assael, and R. A. Perkins. Reference correlation of the thermal conductivity of carbon dioxide from the triple point to 1100 k and up to 200 MPa. Journal of Physical and Chemical Reference Data, 45(1):013102, mar 2016. doi: 10.1063/1.4940892.

[13] John D. Anderson. Computational fluid dynamics the basic with applications. McGraw-Hill, 1995. ISBN 9780071132107.

[14] Stefan Schreier. Compressible flow. Wiley, 1982. ISBN 047105691X.

[15] N. R. Bulley, M. Fattori, A. Meisen, and L. Moyls. Supercritical fluid extraction of vegetable oil seeds. Journal of the American Oil Chemists' Society, 61(8):1362–1365, aug 1984. doi: 10.1007/bf02542243.

[16] M. Spiro and M. Kandiah. Extraction of ginger rhizome: partition constants and other equilibrium properties in organic solvents and in supercritical carbon dioxide. International Journal of Food Science & Technology, 25(5):566–575, jun 2007. doi: 10.1111/j.1365-2621.1990.tb01116.x.

[17] Helena Sovova. Broken-and-intact cell model for supercritical fluid extraction: Its origin and limits. The Journal of Supercritical Fluids, 129:3–8, nov 2017. doi: 10.1016/j.supflu.2017.02.014.

[18] Motonobu Goto, Bhupesh C. Roy, and Tsutomu Hirose. Shrinking-core leaching model for supercritical-fluid extraction. The Journal of Supercritical Fluids, 9(2):128–133, jun 1996. doi: 10.1016/s0896-8446(96)90009-1.

[19] Jürgen Gmehling, Michael Kleiber, Bärbel Kolbe, and Jürgen Rarey. Chemical Thermodynamics for Process Simulation. Wiley, mar 2019. doi: 10.1002/9783527809479.

[20] H. Sovova, R. Komers, J. Kucuera, and J. Jezu. Supercritical carbon dioxide extraction of caraway essential oil. Chemical Engineering Science, 49(15):2499–2505, aug 1994. doi: 10.1016/0009-2509(94)e0058-x.

[21] Robert P. Dickinson and Robert J. Gelinas. Sensitivity analysis of ordinary differential equation systems—a direct method. Journal of Computational Physics, 21(2):123–143, jun 1976. doi: 10.1016/0021-9991(76)90007-3.

[22] Timothy Maly and Linda R. Petzold. Numerical methods and software for sensitivity analysis of differential-algebraic systems. Applied Numerical Mathematics, 20(1-2):57–79, feb 1996. doi: 10.1016/0168-9274(95)00117-4.